Geodetic investigation on the Suban Field, Southern Sumatra

Intern: Xiaopeng Tong
Mentor: Khalid Soofi, Richard Schultz
Collaborator: Bob Krantz, Peter Hennings

Summer 2012

Geological Technology, ConocoPhillips

Part I: Suban Field, South Sumatra: Local surface deformation rates, surface lineaments from InSAR and comparison with subsurface geology

Background

Suban field is a major oil and gas producing field in Southern Sumatra owned by ConocoPhillips Indonesia. This part of the research is to investigate the vertical deformation near the Suban field in Southern Sumatra with the aid of remote sensing techniques. Extraction of oil potentially causes volume reduction or increase of the subsurface, which is manifested by subsidence or uplift at surface. Interferometric Synthetic Aperture Radar (InSAR) on board satellites provides high-resolution and high-precision imagery of ground deformation to reveal the potential vertical motion near the Suban field.

Sumatra is the sixth largest islands of the world. It is part of the island chain that separate the Indian Ocean from the Pacific Ocean. Sumatra Island trends northwest-southeastward, bounded by Sumatra Subduction zone to its west several hundred miles away (figure 1). The Sumatra Subduction zone is infamous for devastating earthquakes and tsunamis. The geological context within the Sumatra island is complex: the Sumatra fault, an inland transform fault over 1000 miles in length, aligns with the island and forms high ridges on its west flank; Active volcanoes sprawling the Sumatra fault amount to as many as 32. Detachment of forearc from the overriding plate causes strain partitioning between the subduction fault and onshore transform Sumatra fault. The back-arc sedimentary basin is deformed by the tectonic movement. Numerous anticline and syncline structures cut through the basin in various directions. The Suban oil field is located within the sedimentary basin to the east of the volcano chains.

This study area is challenging for remote sensing surveys because it is always covered with clouds. The radar onboard satellite is less affected since the microwaves band of the electromagnetic waves can penetrate through the cloud coverage. However the lush tropical vegetations make the ground reflectivity changing rapidly, causing the radar image lose its coherence over 1 or 2 years. In this study we used a new satellite that operated at L-band to mitigate problems due to vegetations. It is possible to install artificial corner reflectors near the Suban field to improve the temporal coherence of the signal.

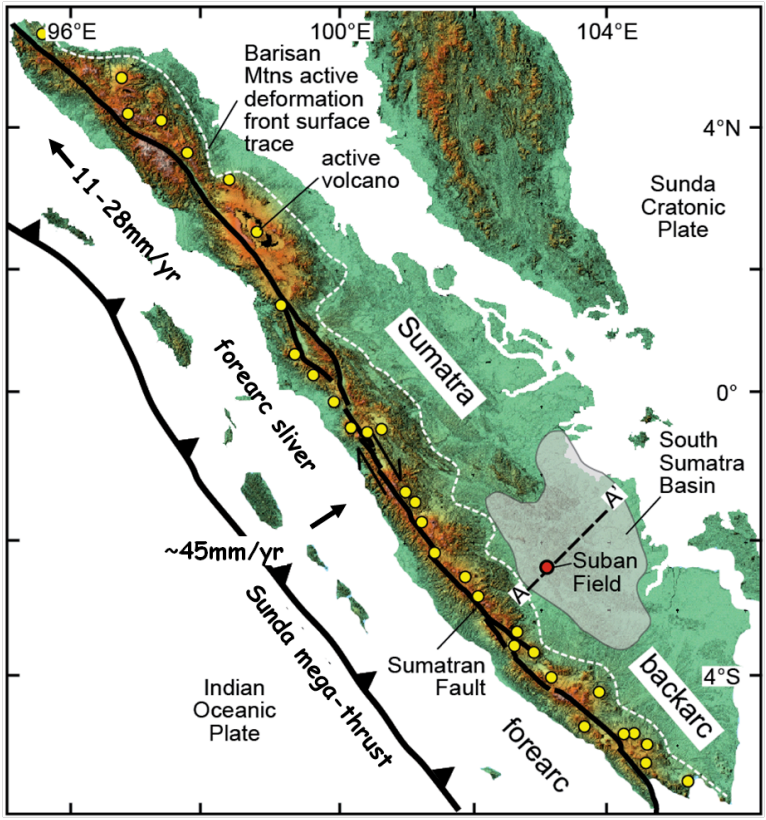

Figure 1. Area of interest. The map shows Sumatra island, the transform Sumatra fault, the Sunda mega-thrust fault and the backarc basin. The Suban oil field is marked. The plate convergence rate is about 60 mm/yr, which can be decomposed into 11-28 mm/yr strike-slip motion along the Sumtra fault and 45 mm/yr thrust motion along the mega-thrust fault.

Data and method

The satellite data used in this study is purchased by ConocoPhillips from Earth Remote Sensing Data Analysis Center (ERSDAC) from Japanese

space agency. The satellite called ALOS carries a L-band radar PALSAR onboard. 26 L1.0 PALSAR raw images are ordered (19 ascending and 7 descending acquisitions) to perform repeat-pass interferometry analysis. This L-band radar operates at 23.6cm wavelength, which is advantageous over the C-band radar (5.6 cm wavelength) in maintaining temporal coherence of the radar images. A good coherence over long time is important to reveal slow ground motion at cm/yr level accuracy. The ALOS satellite was launched in 2006 and collected almost 5 years of data. The first few months of data is not collected over certain areas because ALOS is in a calibration mode. The satellite failed due to power issue in the middle of 2011. The data we ordered ranges from the middle of 2007 to the end of 2010. ALOS ascends in the orientation of 9 degrees west to the north flying at 800 km altitude and illuminating the study area at about 10:30 PM local time. Since the incidence angle is 34.3 degrees from vertical, these interferograms are mainly sensitive to the vertical component of ground motion. Two look directions from both the ascending and the descending orbits are critical to distinguish vertical motion from the horizontal motion. We combined the Line-Of-Sight (LOS) motion measured in two look directions to derive vertical and horizontal deformation maps. Along the descending orbits the satellite collects fewer radar data because of the conflict with other sensors onboard.

The data are processed with GMTSAR software on a Linux platform. In the repeat-pass interferometry analysis, we first pre-processed the raw binary radar images. Next we aligned two images with 2D cross-correlation techniques (figure 2). The image alignment has to be accurate within 1 pixel (~10m) before constructing interferograms. The phase due to topography is removed with digital elevation model SRTM. Then the residual phase is unwrapped with SNAPHU software. The above procedures yield 20 good quality interferograms (figure 3 and 4). These 20 interferograms are visually inspected and checked. These unwrapped phase maps are high-pass filtered individually then stacked to yield an average Line-of-sight (LOS) velocity map of the Suban field (called “stacking” technique). The filtering step reduces the error sources associated with long wavelength characteristics. The filtering wavelength is 20 km thus any ground motion at greater than 20 km wavelength is filtered out. We focus on resolving the small scale ground motion near the Suban field. The stacking analysis improves the signal to noise ratio by averaging the random part of the noise. In general, the more the interferograms used in this analysis, the better the stacking result would be. We calculated the standard deviation of the LOS velocity to evaluate the

uncertainties caused by various error sources, such as clouds in the troposphere, ionosphere delay, inaccurate orbital ephemeris, unwrapping errors (called “noise map”). This standard deviations of the velocity map ranges from 0 to 100 mm/yr and has a mean of 12 mm/yr and a standard deviation of 10 mm/yr, higher than what is found in California by a factor of 4. This larger error is expected because the Suban field is located at a highly vegetated area within the tropical region. We masked out any area in the LOS velocity map with large noise (standard deviation > 20 mm/yr). The final stacked and masked LOS velocity map ranges from -23 to 33 mm/yr approximately with a standard deviation of ~4 mm/yr. We did a similar analysis to the descending data. However, stacking of the descending data is more difficult due to lack of available data. All the results derived from the above analysis are summarized in an ArcGIS map file.

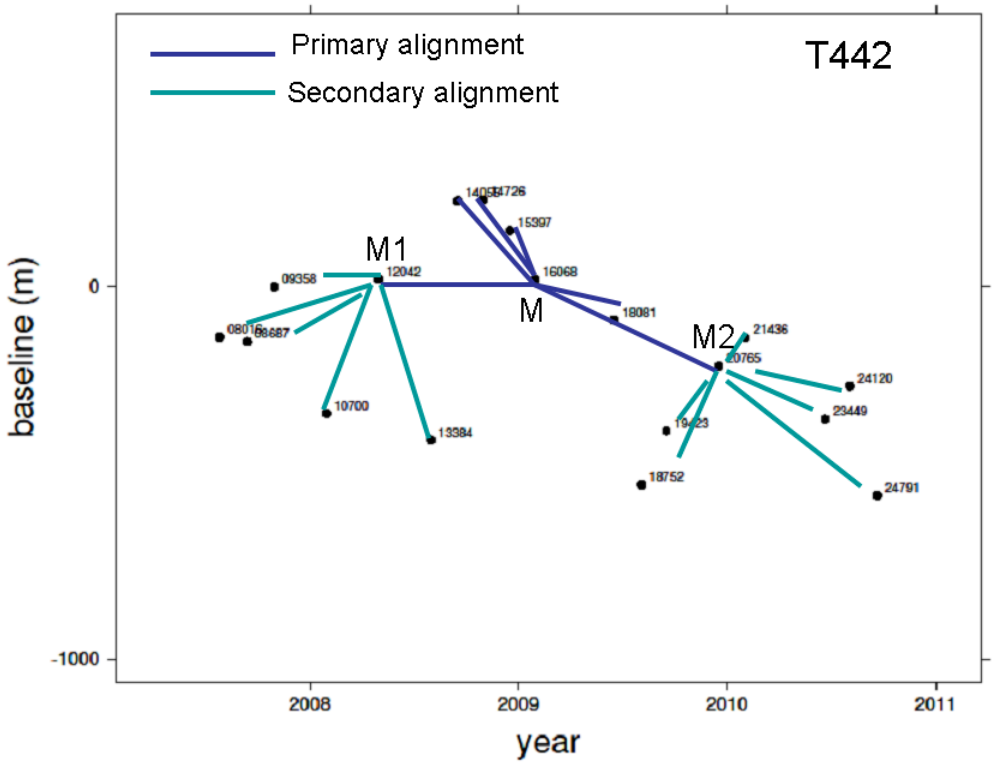
Primary alignment
Secondary alignment
T442
M1
M
M2
baseline (m)
0
-1000
2008
2009
2010
2011
year

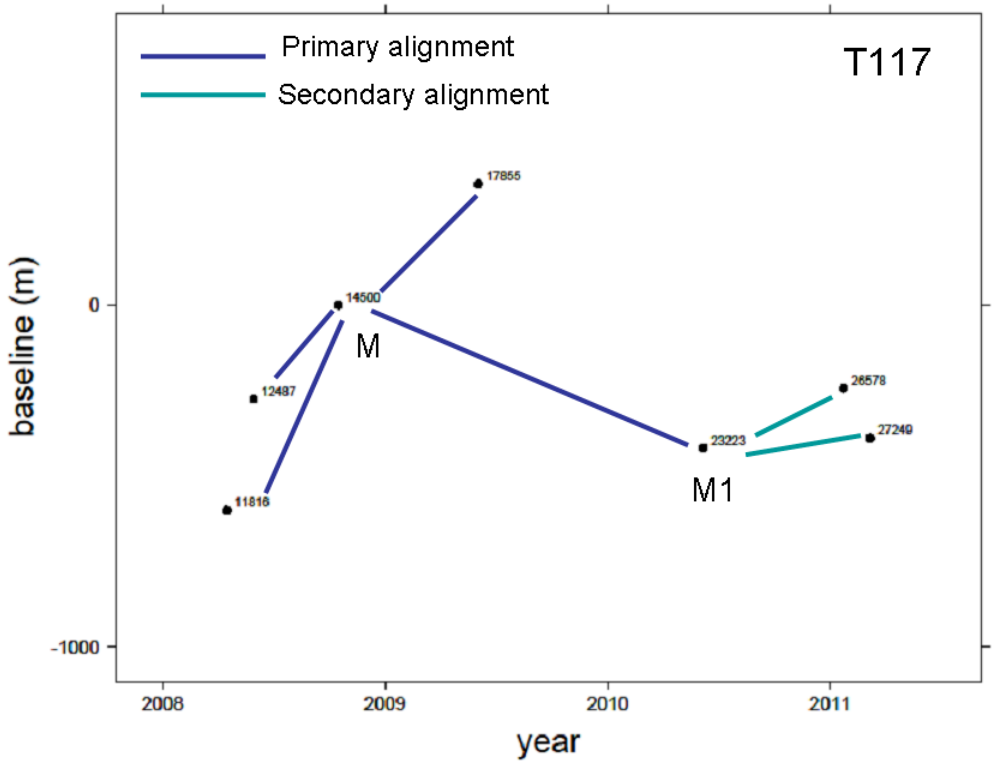
Primary alignment
Secondary alignment
T117
M
M1
baseline (m)
0
-1000
2008
2009
2010
2011
year

Figure 2. Baseline vs. time plots for tracks T442 (ascending) and T117 (descending). The acquisitions are labeled according to orbital revolutions since launch. In figure 2a, there are 18 acquisitions shown in this plot. There is another acquisition but off the map as its baseline is too large. In figure 2b, there are 7 acquisitions as the descending orbits don't acquire radar images as frequent as the ascending orbits. The colored lines show how the images are aligned to one single master image M. M1 and M2 are called "surrogate master". The dark blue lines indicate primary alignments and the light blue lines indicate secondary alignments.

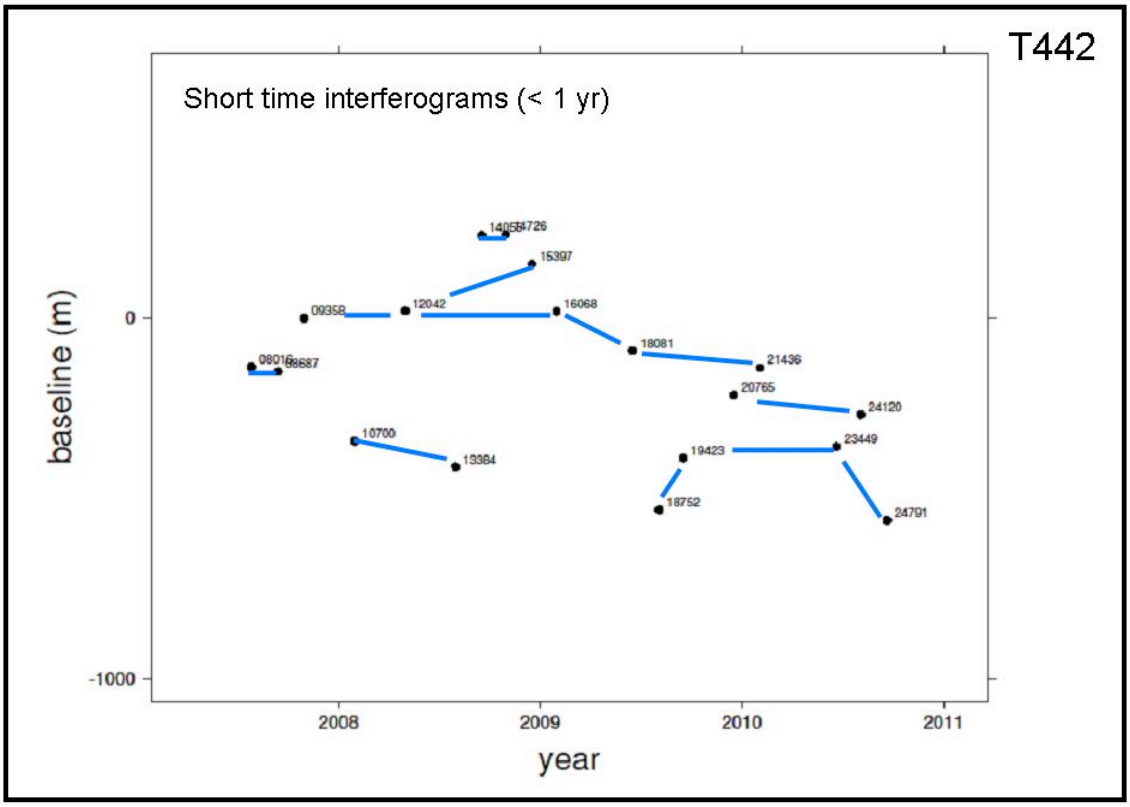
T442
Short time interferograms (< 1 yr)
baseline (m)
0
-1000
2008
2009
2010
2011
year
15397
09358
12042
16068
18081
21436
20765
24120
10700
13384
19423
23449
18752
24791

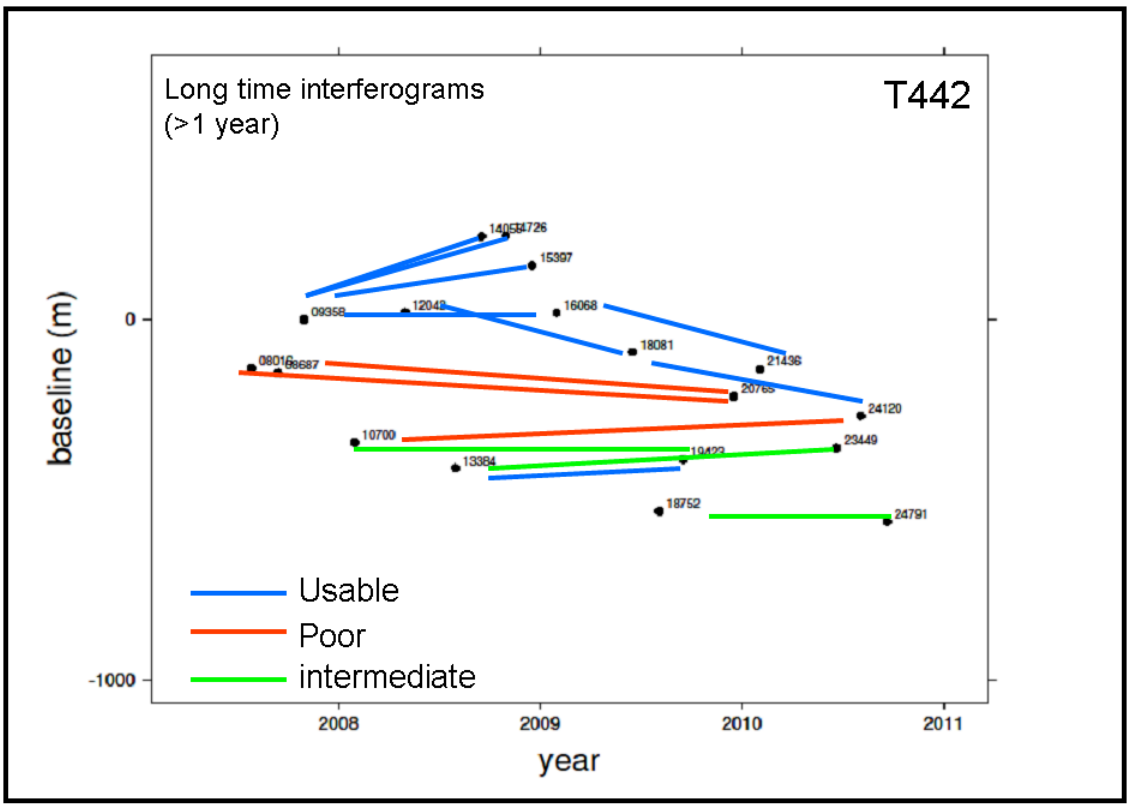

Figure 3. The choice of interferograms for ascending track T442. The top panel shows 12 short time (< 1 year) interferograms and the bottom panel shows the experiment with long time interferograms. Surprisingly some long time (> 1 year) interferograms yield descent correlations. 8 out of 14 long time interferograms are of good quality and was used in conjunction with 12 short time interferograms in the stacking analysis. 3 of 14 interferograms are completely decorrelated due to their greater than 2 year time interval. The other 3 are of intermediate quality but it's difficult to unwrap them correctly.

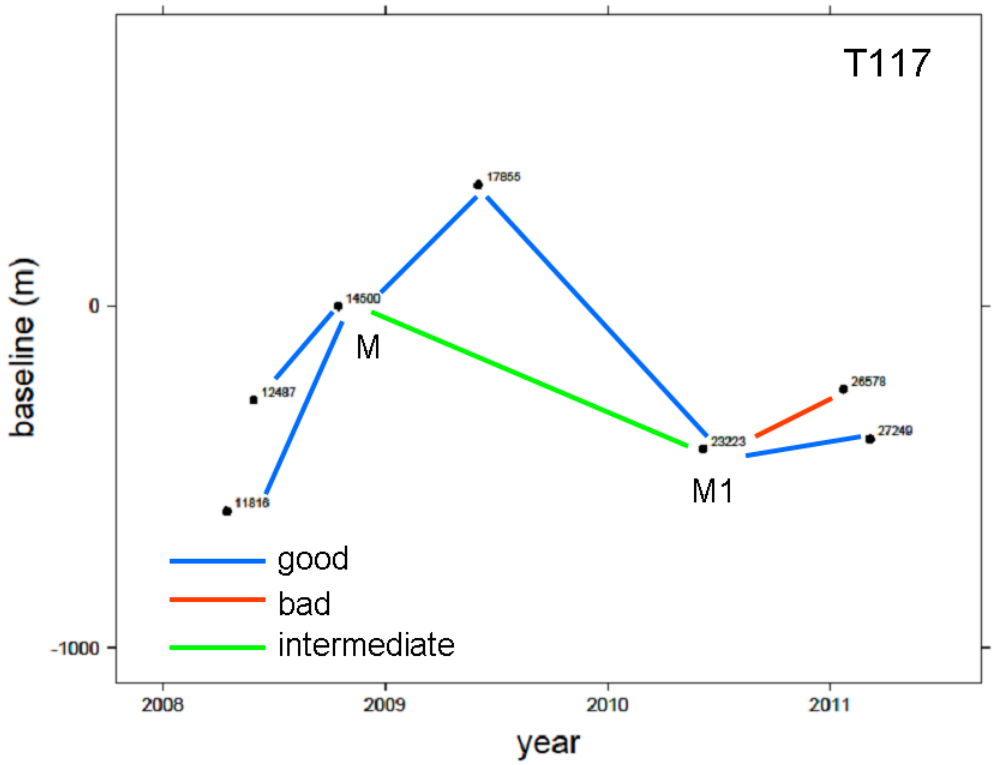

Figure 4. The choice of interferograms for descending track T117. There are 7 interferograms processed in total. 5 out of 7 interferograms are of good quality.

Results

1. Short time interferogram v.s. long time interferogram

Here we demonstrate how the phase and coherence are affected by the time span of the interferogram. As shown in figure 5, an interferogram (08016-08687) spanning 1 orbital cycle, i.e., 46 days, gives excellent coherence and phase signal. The phase is dominated by a trend in the northwest direction, perhaps due to the orbital error and ionosphere/atmosphere noise. In the coherence map the white area shows high coherence and the black area shows low coherence. In contrast, the other interferogram (13384-19423) that spans 9 orbital cycles, i.e., over 1 year, is of low coherence. Its phase is noisier and has interesting "blobs" that might be related to local deformation. One color cycle in the phase map is equivalent to 11.8cm motion in LOS direction.

2. Stacking amplitude

We stacked 20 amplitude images of the interferogram to derive an average amplitude map of this area. In figure 6, the white area shows the ground with strong reflectivity. We suspected a feature with a strong reflectivity within the Suban field to be the main station inside the Suban reservoir. We confirmed this finding by overlying a high resolution (2.5m) SPOT image on top of the ALOS amplitude images. The agreement also verifies that the ALOS images are well registered.

3. High-pass filtered phase

In order to isolate small scale motions and reduce long wavelength noise from the interferograms, we applied the high-pass filtering (20km cut-off wavelength) to the unwrapped interferograms. As shown in figure 7, the LOS motion reaches -10 to 10 mm in this example (12042-15397). The difficulty lies on how to assure these are deformation signal rather than atmosphere noise. We attempted to examine the optical band of the MODIS images onboard AQUA and TERRA satellite to identify cloud coverage over the area. The AQUA and TERRA acquire images over the Suban field in the morning and in the afternoon, several hours apart from the ALOS acquisition along the ascending orbit (10:30PM). We didn't find a way to extract this meteorological dataset to reduce troposphere noise in the interferograms.

4. Stacking

We stacked 14 filtered interferograms along the ascending track and 6 along the descending track to derive an averaged LOS velocity map over the Suban field assuming the deformation rate is linear (Figure 8). In addition we calculated the standard deviation of the LOS velocity to evaluate the uncertainties caused by various error sources (Figure 9). We found that removing 6 short time (e.g. 1 or 2 months interval) interferograms along the ascending orbits helped reduce noise in the LOS velocity map. The standard deviation of the ascending LOS velocity exceeds 20 mm/yr over certain regions in the Suban Field. This larger error is expected because the Suban Field is located at a highly vegetated area within the tropical region. We masked out any area in the LOS velocity map with large noise. As discussed

in the later section we found that the regions with interesting deformation patterns are located in the area of relatively low noise.

5. Vertical and horizontal velocity

For any ground point, the LOS velocity is simply a projection of the east-north-up velocity components. The projection is based on the azimuth of the satellite trajectory (8 degrees counter-clockwise from north for ALOS) and the look angle of the radar. If we take the look angle of the radar to be constant (34 degrees for ALOS), we get:

$$V_{asc} = 0.61V_{East} + 0.13V_{North} - 0.79V_{Up} \quad (1)$$
$$V_{des} = -0.61V_{East} + 0.13V_{North} - 0.79V_{Up} \quad (2)$$

We used the above formulas and neglected the north component of the velocity to derive vertical and east components from the ascending and descending LOS velocity maps. The north component only contributes 13% to the LOS velocity thus the LOS velocity is not so sensitive to the north component as to the east and vertical components. We conducted a test to investigate whether assuming the northward velocity to be zero would influence the results. Instead of taking V_{North} to be zero, we assume it's the same as the V_{East}. In other words, the horizontal motion is in NE direction. We found that the result is similar to the previous results, which means that the east and vertical rates we obtained here are reliable. This issue can be further validated by installing in-situ GPS sites within the Suban Field.

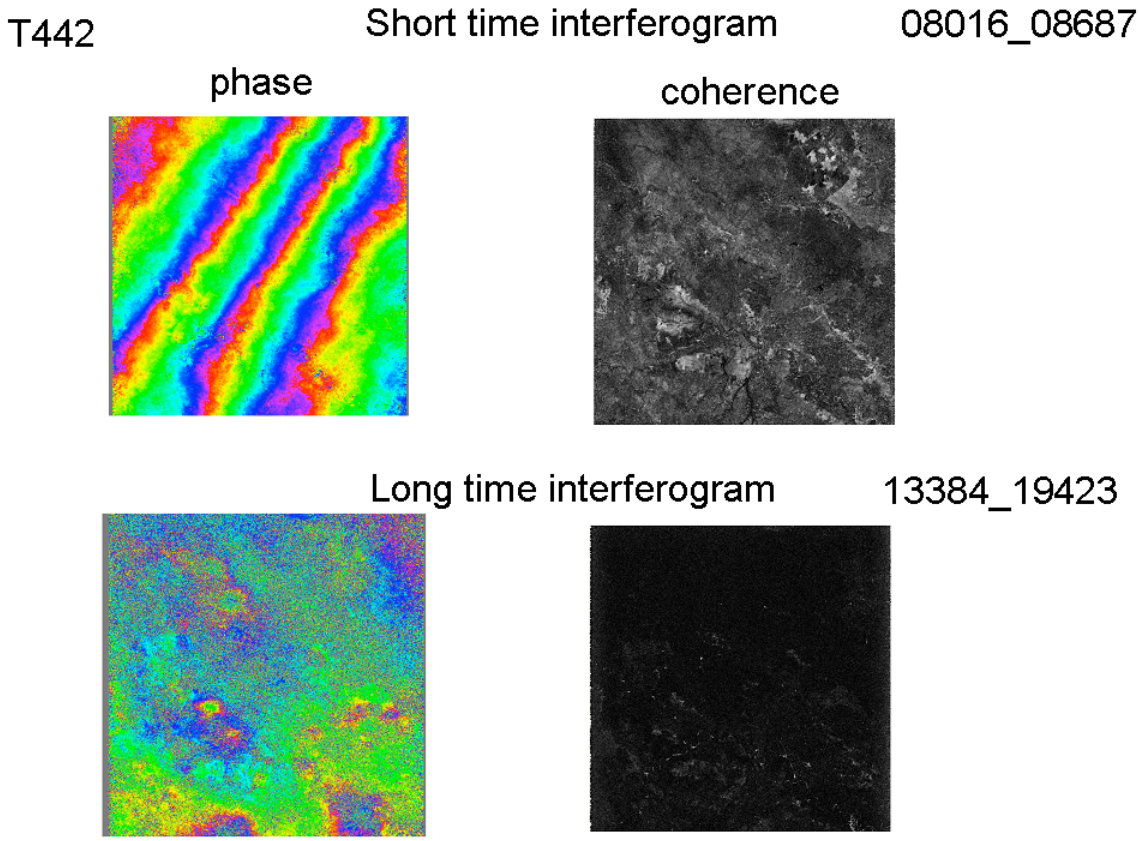

Figure 5. Comparison of short time interferogram with long time interferogram. One color cycle in the phase map is equivalent to 11.8cm motion in LOS direction. In the coherence map the white area shows high coherence and the black area shows low coherence.

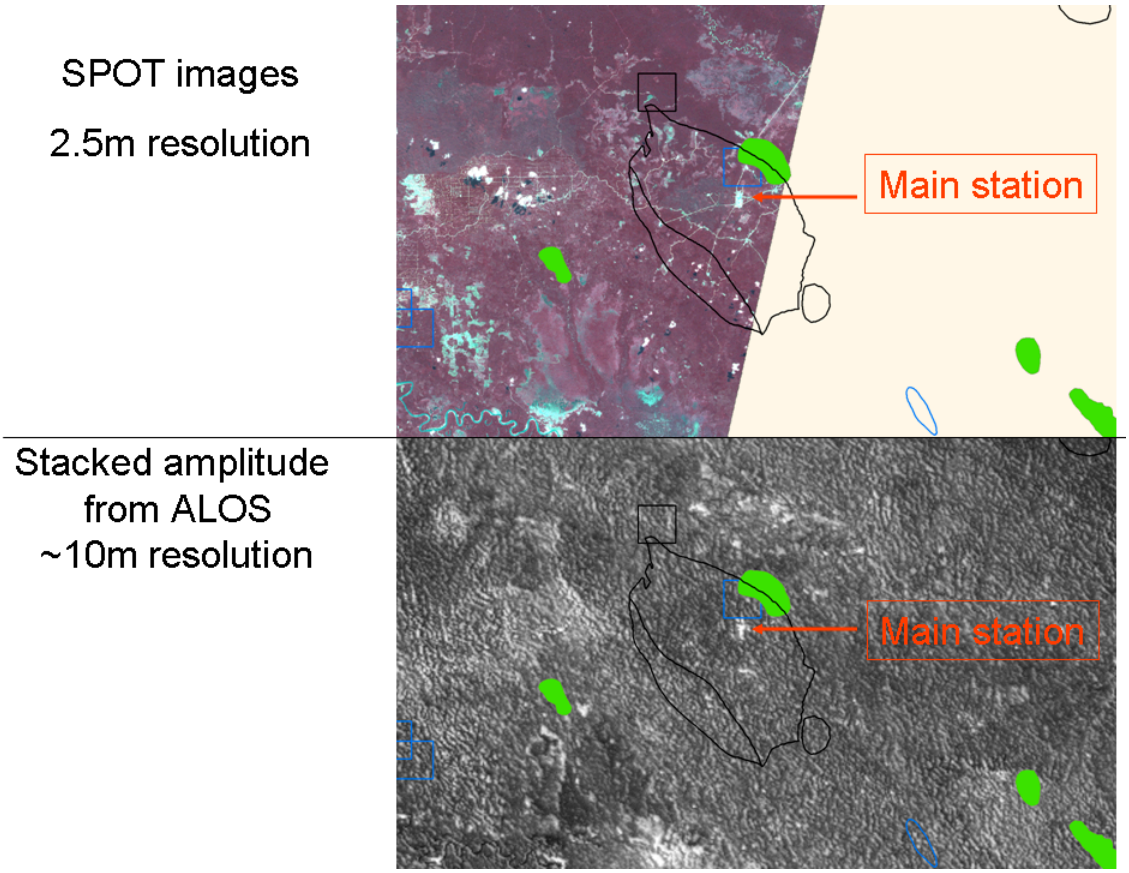

Figure 6. SPOT images and the stacked amplitude images. The main station is marked by the red arrow. The black lines are the Suban reservoir. The green, black, and blue blobs are oil and gas fields.

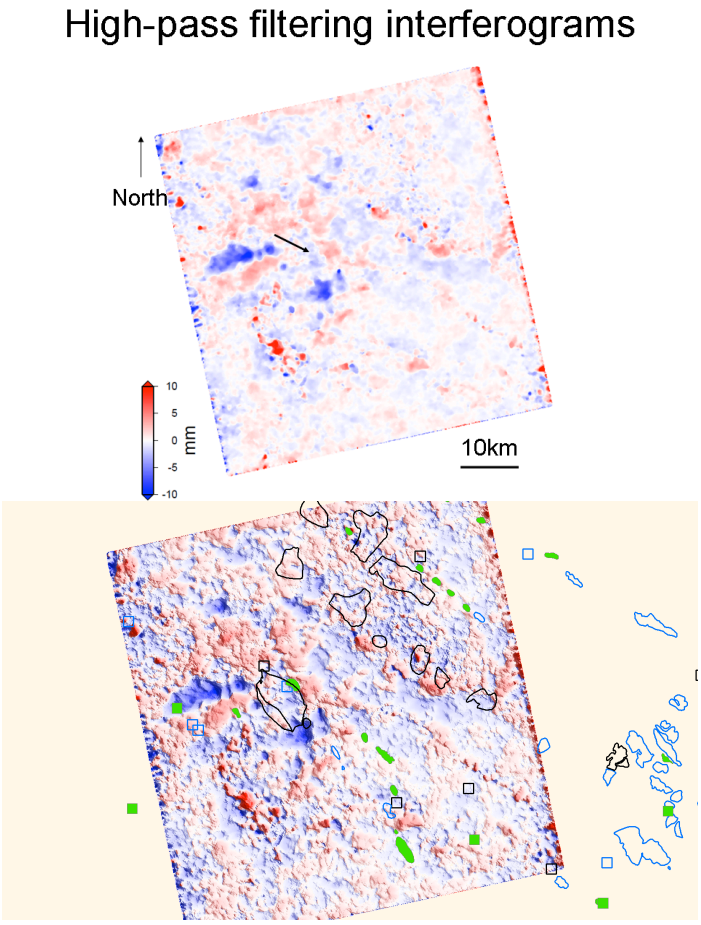

Figure 7. Filtered interferogram. The LOS motion reaches -10 to 10 mm in this example (12042-15397).

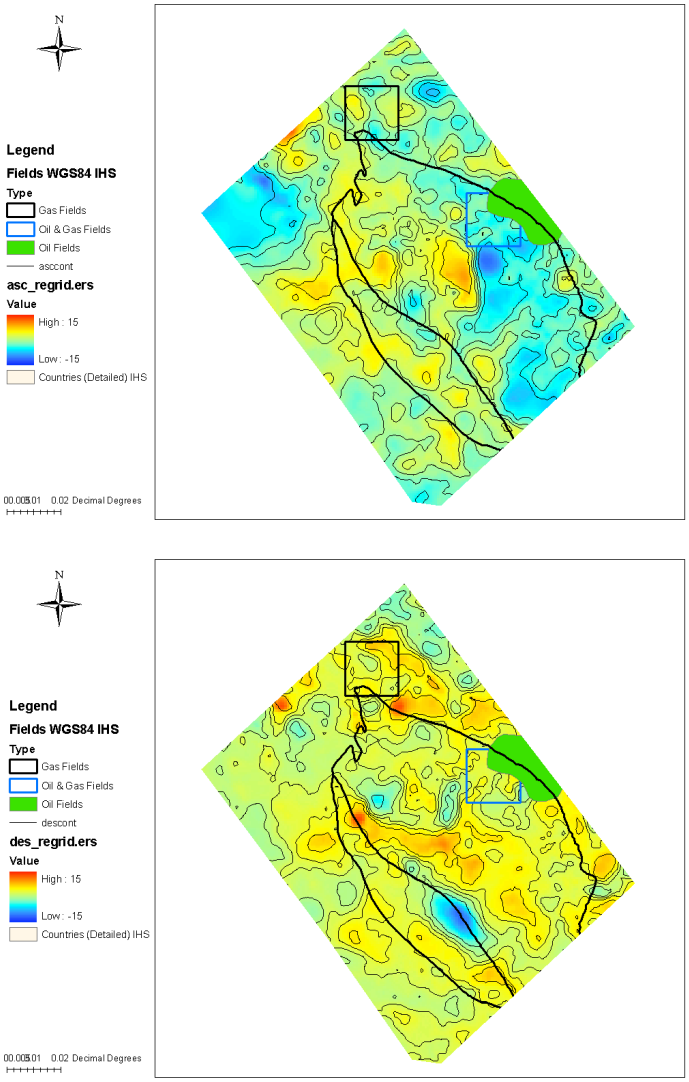

Figure 8. Stacked LOS velocity map. We stacked and filtered the unwrapped phase images to derive an averaged LOS velocity map over the Suban field assuming the deformation rate is linear. Top panel shows the LOS velocity along ascending orbit and the bottom panel shows the LOS velocity along the descending orbit. The thin black contours are at 5mm/yr interval.

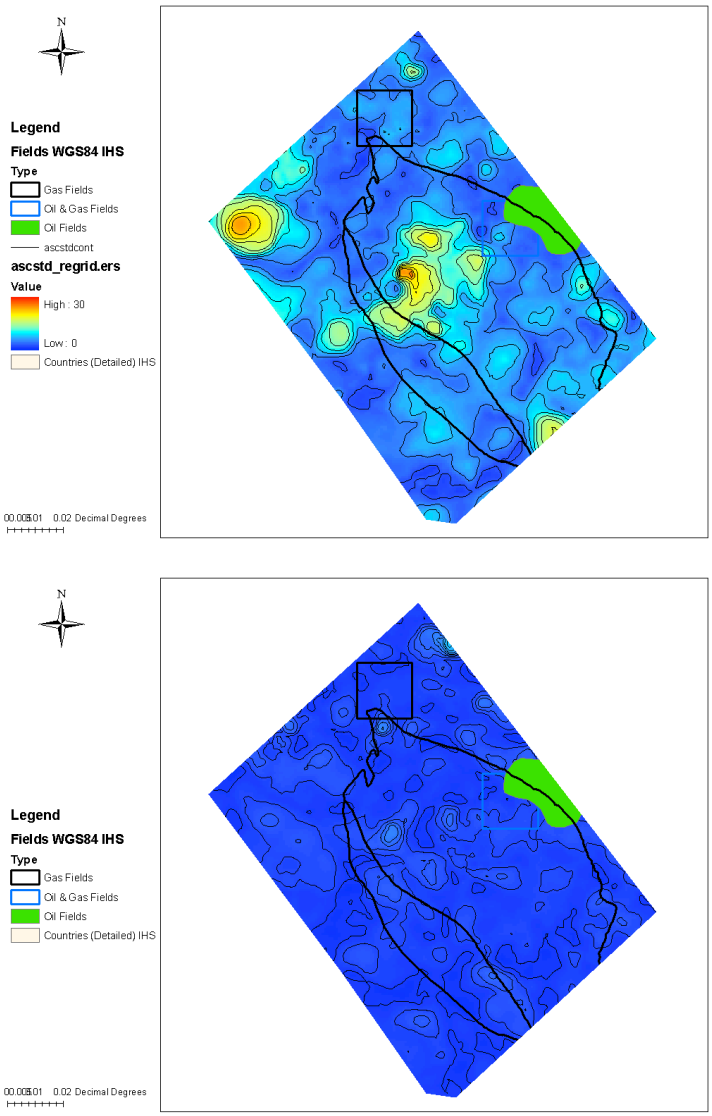

Figure 9. Noise of the LOS velocity map. We calculated the standard deviation of the LOS velocity to evaluate the uncertainties caused by various error sources. The contours are at 5 mm/yr interval. The top panel shows the standard deviations of the ascending LOS velocity and the bottom panel shows the standard deviations of the descending LOS velocity.

Discussion

Since the fluid is being extracted from the oil reservoir one might expect a simple subsidence confined by the oil platform. Surprisingly we found a complicated pattern of deformation signal. There are both uplift and subsidence within or near the Suban field. We have not completely understood this phenomenon yet. Fluid injection and extraction are of primary concerns but the structure within the sedimentary basin could also lead to deformation inhomogeneities. To investigate the deformation map in detail, first we analyzed the lineaments from the deformation map and compared them to the previous study (Corridor work, 2004). Second, we distinguished and quantified different deformation patterns, such as compression, subsidence and uplift in the Suban Field. We further investigated the deformation map by integrating subsurface structure data from seismic imaging study.

1. Lineaments analysis

We compared the lineaments from our deformation analysis with previously mapped surface lineaments (Hennings/Krantz/Soofi/Flanagan/Zahm/Reid Jr). To the first order the orientation of the lineaments are in NW direction, similar to the previous study (Figure 10). Some lineaments even overlapped with previous lineaments, suggesting that those lineaments are currently active.

2. Regions of compression, subsidence and uplift and comparison with the subsurface faults

We found a region of compression in the center of the Suban Field from the east velocity map (Figure 11). It is interesting because this compression is expected from regional compression in the NE-SW direction. The vertical rates map shows 3 areas of subsidence located in the center and west of the Field. The subsidence exceeds 10 mm/yr in the center (Figure 11). The subsidence could be led by the influx of aquifer fluids due to depletion of gas or other regional effects (e.g. Surmont) Besides subsidence we found 2 areas of uplift. There is an abrupt uplift on the west flank of the Suban Field that correlates with subsurface faults mapped by COP (Figure 12). This uplift region is elongated in the NW direction, similar to the trend of the faults. The subsurface faults consist of the main oblique thrust fault (SW

fault) and numerous secondary faults. We expect this uplift is controlled by the subsurface fault under regional and local stress. If the main thrust fault is creeping aseismically, we expect uplift or perhaps folding on the hanging wall side of the fault. On the other hand, the fault zone material might also experience inelastic deformation because of the presence of fractures. More InSAR/GPS data are needed to confirm this intriguing deformation pattern. There is a gradual uplift on the east of the Field that can be related to the anticline within the Field.

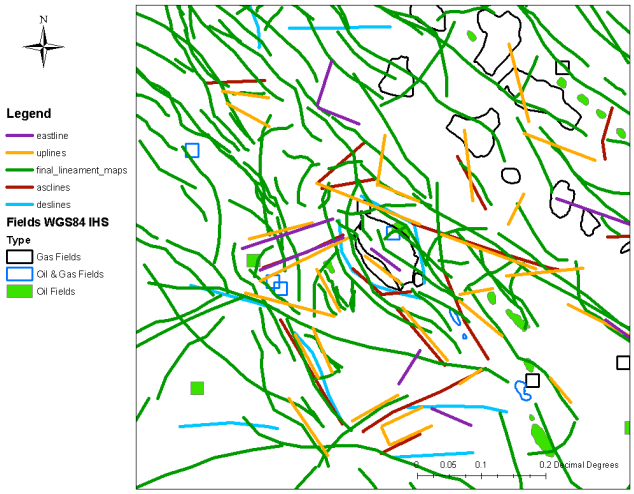

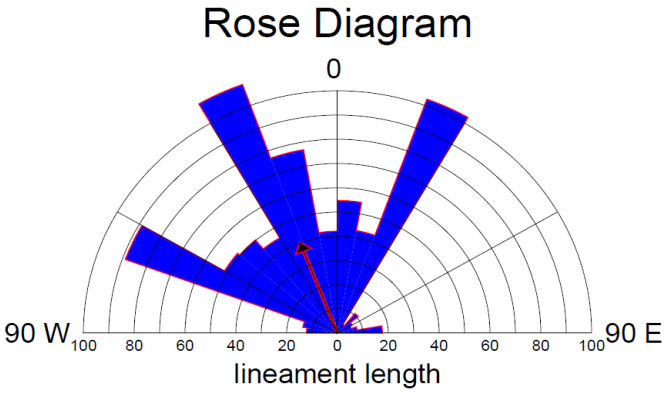

Figure 10. Lineaments analysis on the deformation map. In the top panel the green lines are the lineaments derived from previous study, and the colored lines are from the deformation map. The bottom panel shows the rose diagram of the lineaments.

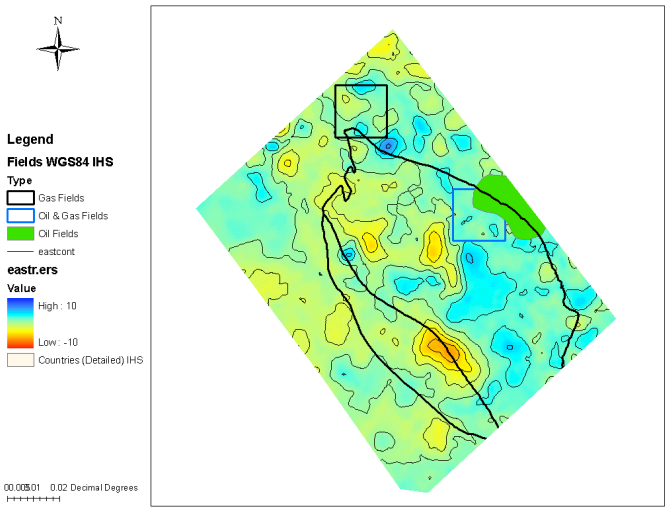

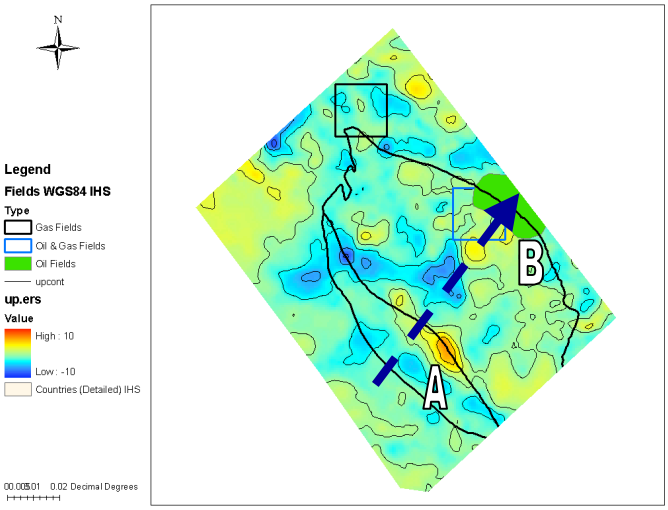

Figure 11. East (top panel) and vertical (bottom panel) velocity map. The contours are at 5 mm/yr interval. Two prominent uplift areas are marked as "A" and "B" and the location of a profile is marked in the vertical velocity map.

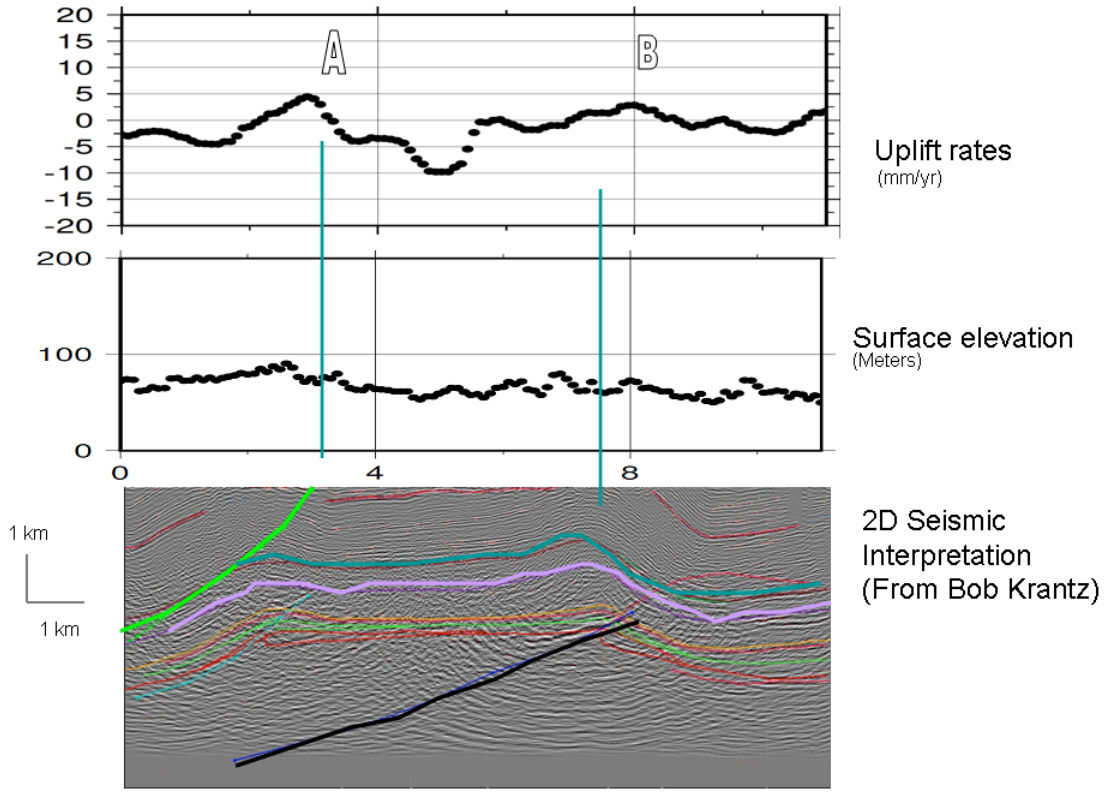

Figure 12. A comparison among surface uplift rates, surface elevation, and 2D seismic interpretations along the same transection across the Suban Field. In the 2D seismic interpretations the bright green line shows the main thrust fault, which correlates with an abrupt uplift region in the deformation map.

Part II: Regional crust deformation of Sumatra from GPS observations

Introduction

The Suban Field is located in the central-south Sumatra, which is 100 miles away from the active tectonic deformation front. The subduction of the Indo-Australia plate and the detachment of the forearc lead to complexity in the kinematics and deformation of Sumatra. Nowadays the mm-scale

deformation can be investigated by Global Positioning System (GPS) observations (Figure 13).

In this part of the work, we will show the regional scale interseismic deformation of Central and South Sumatra. The GPS data used in our study comes from continuous sites from SuGAr and survey sites from 2001-2007. We used DEFNODE to model the secular GPS velocity and uplift rates from coral record. We attribute the tectonic deformation to rotation of rigid individual blocks and interseismic locking on the block-bounding faults. We take account for the Subduction fault offshore and the transform fault onshore. There are 3 blocks: Sunda, forearc, Indo-Australia in this model (Figure 14).

DEFNODE is a Fortran 77 program to study the plate coupling and crustal block rotations [McCaffrey, 2007]. We designed a control file to specify the model parameters. This model can take data input such as GPS vectors, surface uplift rates from coral records, long-term fault slip rates and solve for the fraction of interseismic locking, block angular velocity and internal strain rates within each blocks. Both forward modeling and inverse modeling can be done with this model.

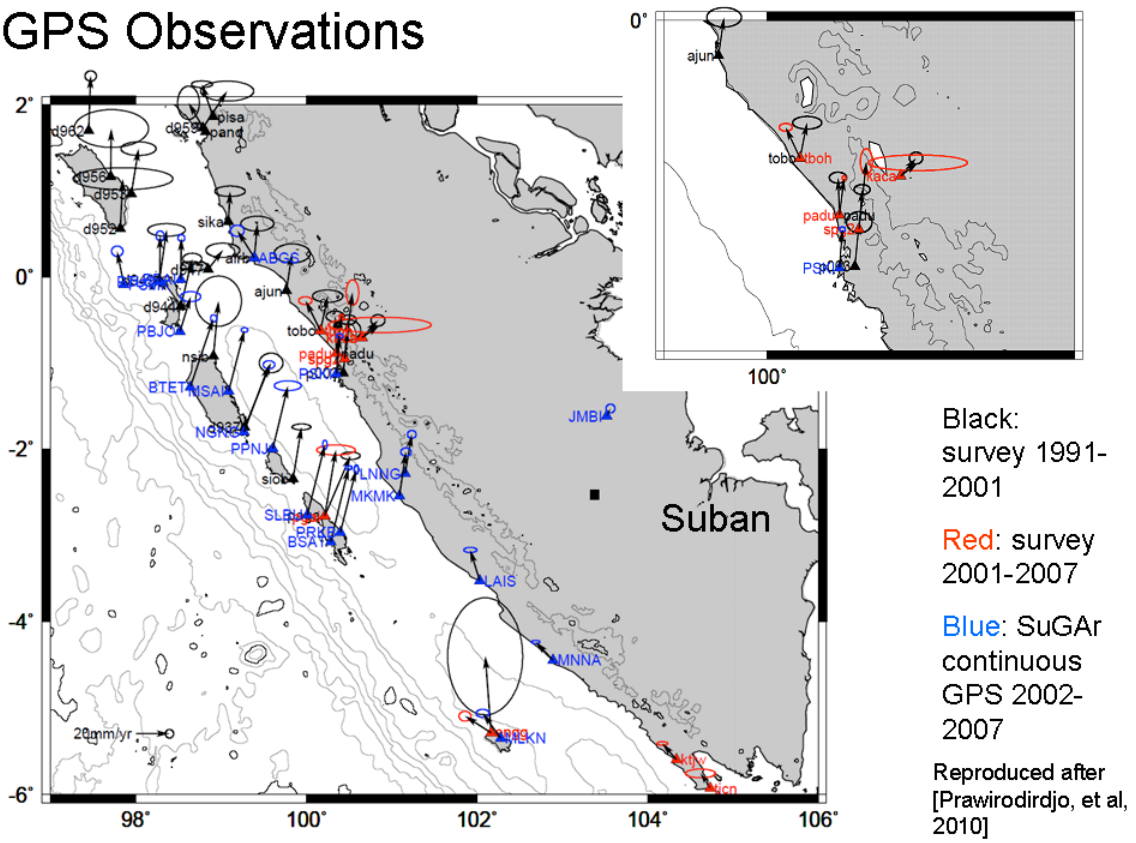

Figure 13. GPS data in Sumatra. The black, red and blue colors represent the secular horizontal velocity from 3 different sources. A change in GPS obliquity can be found in this map, which could reveal a change in the slip partitioning taken up by the forearc block, or a change in plate coupling as interpreted by Prawirodirdjo et al. [2010].

Preliminary result

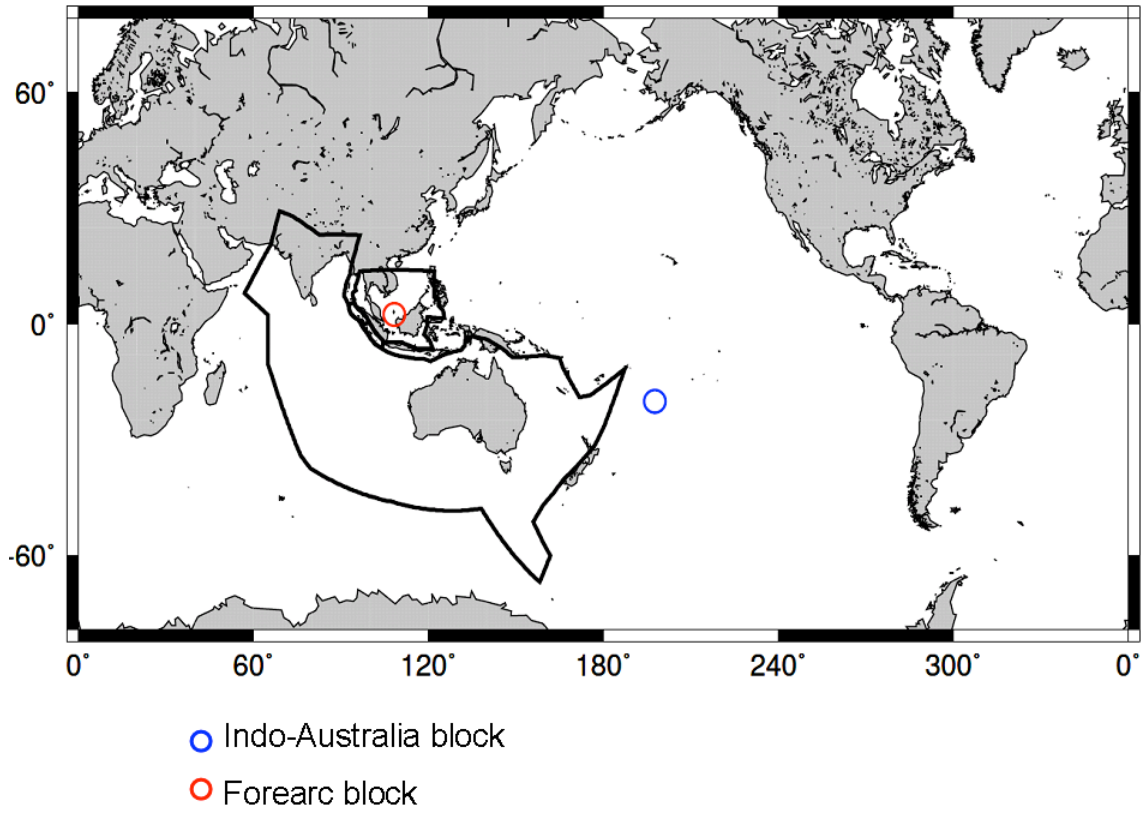

Figure 14. Rotation pole for blocks. The blue color is the pole for the Indo-Australia block and the red one is for the forearc block.

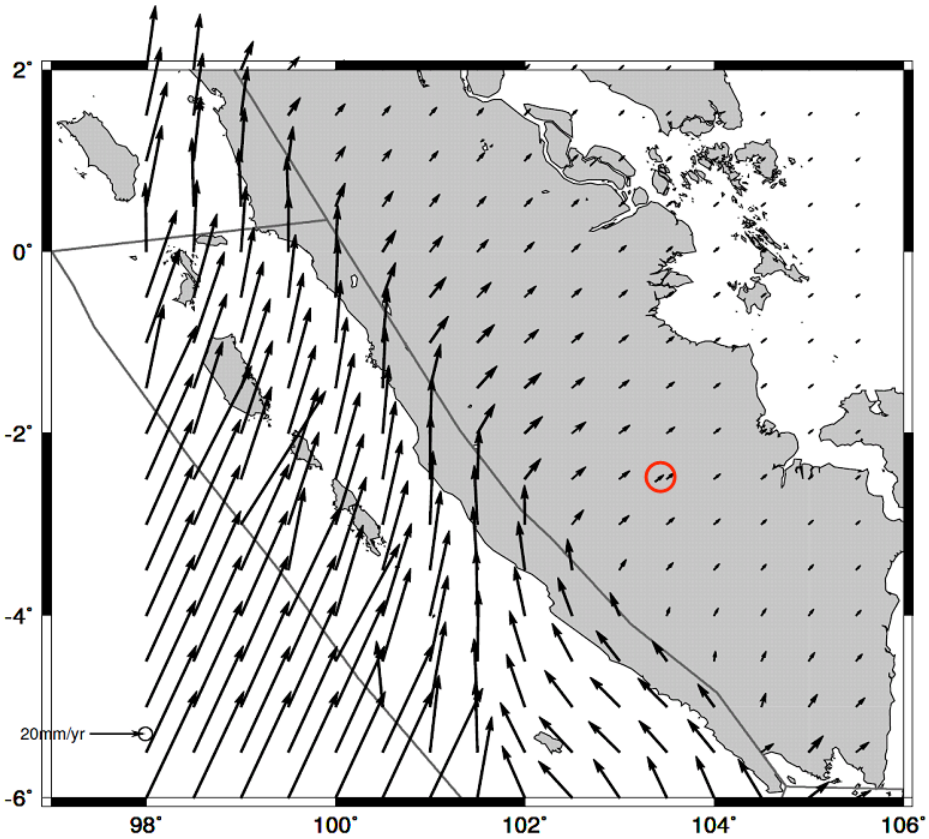

Figure 15. Horizontal velocity field predicted by the "block model". The thin black lines are the block boundaries. The red color marks the Suban field, which moves at 4 mm/yr in NE.

Conclusions

1. We assessed the viability of the InSAR technique over a highly vegetated area in South Sumatra. We found that L-band InSAR processing aboard satellites over Suban Field is feasible.

2. We have constructed vertical and horizontal velocity rate map of the Suban Field. The velocity rates can vary from -10 to 10 mm/yr. Complex patterns of subsidence and uplift are found within the Field. The Suban Field is actively deforming.

3. Analysis suggests that the deformation lineaments are mainly in northwest-southeast with a deviation in NS and WNW. To first order,

the result is in agreement with previous lineaments studies, also consistent with a NE-SW compressive stress field.

4. Comparison with Subsurface faults from 2D seismic interpretations suggests a positive spatial correlation of surface deformation and faults.

5. We related the local deformation of Suban to regional kinematic framework of Sumatra using models based on GPS data.